Pergamon

Int. J. Heat Mass Transfer. Vol. 37, No. 8, pp. 1207–1216, 1994

0017-9310/94 $7.00 + 0.00

0017-9310(93)E0031-B

Local heat transfer to impinging liquid jets in the initially laminar, transitional, and turbulent regimes

B. ELISON† and B. W. WEBB‡

Department of Mechanical Engineering, Brigham Young University, Provo, UT 84602, U.S.A.

(*Received* 13 *August* 1993 *and in final form* 29 *October* 1993)

Abstract—Transport from small diameter, fully-developed liquid jets impinging normally on a constant heat flux surface has been investigated. This study focuses on jet Reynolds numbers spanning the laminar, transitional, and turbulent flow regimes at the nozzle exit, $300 \leqslant Re \leqslant 7000$. Jet diameters studied include 0.584, 0.315, and 0.246 mm. Both free-surface and submerged jets were studied. Local heat transfer coefficient information was collected, and the radial variation of the Nusselt number is explored. Correlations of stagnation Nusselt number as a function of Reynolds number for laminar and turbulent data are presented. The Nusselt number was observed to correlate approximately with $Re^{0.5}$ and $Re^{0.8}$ for initially turbulent and laminar jets, respectively. This dependence was observed for both free-surface and submerged jet configurations. The $Re^{0.8}$ dependence of the Nusselt number in the laminar regime for free-surface jets is attributed to surface tension-induced jet broadening at the jet exit. For the submerged jet the $Nu_0 \sim Re^{0.8}$ laminar regime functionality is explained by the dominating effects of jet destabilization. The free-surface configuration heat transfer data showed little dependence on nozzle-plate spacing. By contrast, the submerged jet data exhibit the usual potential core behavior for turbulent flow with its well-established dependence on nozzle-to-plate spacing. The Nusselt number was seen to be independent of nozzle-to-plate spacing in the initially laminar jet regime.

INTRODUCTION

LIQUID jet impingement heat transfer has been the subject of intense study recently in the heat transfer community. This interest is motivated by the very high local heat transfer coefficients that can be achieved using impinging jets. Applications of liquid jet impingement heat transfer include localized cooling in internal combustion engines, quenching of metals and other materials in manufacturing processes, and thermal control of high performance computer components.

Two types of single-phase jets have been studied in the literature: submerged liquid jets and free-surface liquid jets. Submerged jets feature the nozzle and heated surface immersed in the impinging fluid. Free-surface liquid jets travel through the ambient gas to strike the heated surface. As a result, free-surface jets may be subject to surface tension effects, and exhibit a flow structure that may include a hydraulic jump.

There is considerable recent experimental work dealing with the heat transfer under impinging circular liquid jets [1–10]. These studies have focused largely on Reynolds number ranges for which the flow at the jet exit is fully turbulent. Only the studies of Womac *et al.* [7] and Ma *et al.* [8] have penetrated the range where the jets were initially laminar ($Re \lesssim 2000$). Further, nozzle diameters in these previous studies were all greater than 1.0 mm, with the exception of the work by Womac *et al.* [7] which included data for $d = 0.457$ mm.

A recent analytical study investigated the effect of surface tension on the heat transfer from laminar, free-surface liquid jets [11]. The analysis revealed that surface tension has the effect of increasing the stagnation point heat transfer coefficient. Slight increases ($< 13\%$) in stagnation Nusselt number for jets characterized by low Weber number were predicted. This was attributed to surface tension-induced free-surface deflection and acceleration of the preimpingement jet.

In many industrial applications utilizing liquid jet impingement heat transfer it is advantageous to maintain low flow rates. Consequently, there is incentive to use very small nozzles and correspondingly low jet Reynolds numbers. As outlined in the foregoing paragraphs, previous studies have focused on heat transfer under turbulent impinging liquid jets with large diameters and high Reynolds numbers. The purpose of this study was to investigate the local heat transfer characteristics of small diameter liquid jets from laminar flow through transition to fully turbulent flow (at the nozzle exit). No previous investigation has fully explored and characterized this regime. Study emphasis was for Reynolds numbers below 7000 using water as the working fluid for both free-surface and submerged jets.

† Currently at IBM, Rochester, MN, U.S.A.
‡ To whom correspondence should be addressed.

NOMENCLATURE

d	inside diameter of nozzle	T_s	local heated plate temperature
Fr	Froude number at the jet exit, $V_j/\sqrt{(gd)}$	T_j	jet liquid temperature
h	local heat transfer coefficient	V_j	average jet exit velocity
h_o	stagnation heat transfer coefficient	We	Weber number, $\rho V_j^2 d/\sigma$
k	liquid thermal conductivity	z	nozzle-to-plate spacing.
L	length of nozzle		
Nu	local Nusselt number		
Nu_o	stagnation Nusselt number	Greek symbols	
Q	volume flow rate of liquid	ν	kinematic viscosity
q''	heat flux	ρ	density
Re	jet Reynolds number, $\rho Q/\pi\nu d$	σ	coefficient of surface tension.

METHOD AND EXPERIMENTAL APPARATUS

Fluid delivery system

The test apparatus is illustrated schematically in Fig. 1. Generally, the fluid delivery system consisted of a constant-pressure, metered supply of working fluid, filter, and nozzle. Distilled water was used in order to avoid corrosion and deposition on the small diameter nozzles, thereby altering their flow characteristics. To prevent fluctuations in the low flow rates investigated, it was important to maintain a constant supply pressure. A large capacity accumulator was thus employed. The accumulator was designed to maintain constant flow rate over the duration of the tests. A 1 μm contaminant filter was included in the flow circuit to prevent small diameter nozzles from clogging during testing. Precision rotameters, in a parallel flow circuit, were used to measure flow rate and could be switched in or out of use by a needle valve at the base of each flow meter. Accuracy of the flow rate from this system is estimated to be $\pm 5\%$.

The nozzles for this study were made by modifying hypodermic needles. The sharp point of the needle was ground to provide a square end. Unfortunately, the grinding process was found to spread metal burs over the nozzle exit. To remedy this problem a two-step operation was adopted to debur the nozzle exit. First, the nozzle was carefully hand ground using emery cloth to remove the majority of the excess metal. Second, a small drill bit was rotated in the exit to detach any remaining lip or bur. The second step of the deburring process resulted in a 120 degree included angle on the interior of the needle exit. Since the nozzles were designed to be long enough to achieve fully-developed flow for most tests, this slight expansion at the nozzle exit is not expected to affect the velocity distribution significantly. After a nozzle had been prepared it was inspected under a toolmaker's microscope to determine inside diameter and the quality of the deburred exit. The nozzles were re-examined after the experiments to ensure that no corrosion or deposition had occurred. Three nozzles of diameter 0.25, 0.32, and 0.58 mm were investigated. The corresponding nozzle length-to-diameter ratios were, respectively, $L/d = 40$, 75, and 67. Using the laminar flow development criterion $L/d = 0.05Re$, the maximum laminar Reynolds number possible while still achieving fully-developed flow was 1340, 1500, and 800 for the 0.25, 0.32, and 0.58 mm diameter nozzle, respectively. Development lengths are expected to be shorter for the fully turbulent nozzle exit conditions. To allow nozzles to be easily interchanged, a gland flange style nozzle retainer was fabricated. A hose barb connected to the liquid supply tubing was attached to a tapered plastic syringe insert. By tightening socket head screws in a gland flange the tapered plastic insert was pressed into the nozzle entry to form a tight seal. The nozzle retainer assembly facilitated periodic inspection or interchange of the nozzles.

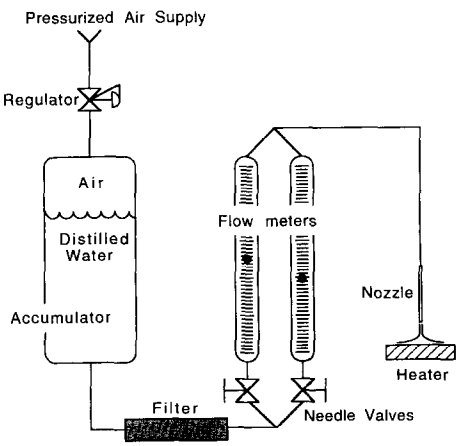

FIG. 1. Schematic diagram of experimental apparatus.

With such low jet Reynolds numbers investigated in the study the possibility of gravitational acceleration was a concern. Bernoulli's equation describes the acceleration of the jet as it leaves the nozzle at velocity V_j and reaches the plate at nozzle-to-plate spacing z with velocity V_p:

$$V_p = (V_j^2 + 2gz)^{1/2}. \quad (1)$$

Equation (1) coupled with the global continuity equation yields a relation for the ratio of Reynolds num-

bers at the plate and jet exit, Re_p/Re. The Reynolds number at the plate is defined in terms of the velocity and corresponding gravity-induced jet contraction diameter for the nozzle-to-plate spacing studied, $Re_p = V_p d_p/\nu$. This ratio expression is

$$Re_p/Re = [1+2(z/d)/Fr^2]^{1/4} \quad (2)$$

where Fr is the Froude number at the jet exit, $Fr = V_j/\sqrt{(gd)}$. For the conditions of this study, the maximum value of $2(z/d)/Fr^2$ was 0.021 for all tests, yielding a maximum difference between Reynolds numbers at the jet exit and the plate due to gravitational effects of 1.8%. Hence, gravitational contraction of the jets was considered negligible.

In order to investigate the local behavior of the impinging liquid jets it was necessary to accurately position the jet in three-dimensional space. A three-axis positioning table was constructed to move the nozzle relative to the heater module. Translation in the horizontal plane was achieved by spring-loaded micrometer-driven stages. These stages provided independent positioning capability in two orthogonal directions in the horizontal plane. Vertical adjustment of the nozzle assembly was effected by a rack and pinion with dial indicator, permitting precise establishment of the nozzle-to-plate spacing. All three axes could be positioned with accuracy of approximately ± 0.013 mm. The positioning apparatus was used (i) to determine the precise location of the stagnation point (by a systematic search for the minimum heated foil temperature), and (ii) to index the position of the jet relative to the stagnation point for the characterization of the radial variation in heat transfer coefficient.

Heater assembly

The heater assembly consisted of a thin metallic foil which was heated Ohmically, thus achieving a constant heat flux thermal boundary condition. Measurement of the surface temperature permitted determination of the local heat transfer coefficient from Newton's law of cooling

$$h = q''/(T_s - T_j) \quad (3)$$

where h is the local heat transfer coefficient, q'' is the imposed heat flux, T_s is the local heated surface temperature, and T_j is the temperature of the liquid jet. The temperature of the impinging liquid was measured by inserting a thermocouple into the water supply line. Thus, to evaluate the heat transfer coefficient the heater assembly was to provide a means of accurately measuring the temperature of the heated plate and the heat flux. This is now described.

Figure 2 shows the heater assembly used in the experiments. A 0.025 mm thick strip of stainless steel shim stock, 6.4 mm in width was stretched tightly over and clamped to large contoured copper bus bars. The distance between the copper bus bars (and, therefore, the length of the foil heated region) was imposed by a machined acrylic spacer as shown in Fig. 2. Very thin

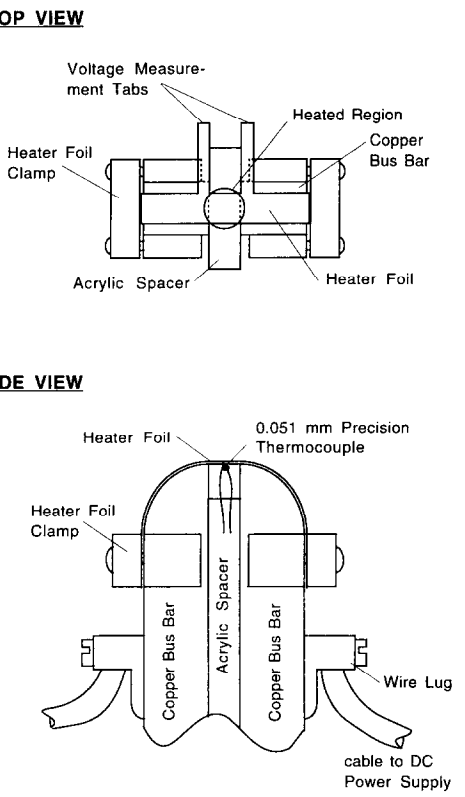

FIG. 2. Detailed schematic of heater assembly.

voltage measurement tabs were fabricated integral to the metallic strip, enabling measurement of the voltage drop (required for determination of the electrical dissipation in the foil) without the uncertainty of electrical contact resistance. The voltage tabs were separated a distance equal to the gap between the contoured bus bars with their inner edges (edges nearest the heated section) exactly flush with the corresponding inner surface of the copper bus bars. Thus, when the heater foil was mounted on the bus bars the voltage tabs did not extend into the electrically heated region of the foil. Careful measurements (using a precision multimeter) of voltage along the width of the integral voltage tabs showed that the voltage was uniform. This test confirmed that voltage data collected from the heater would accurately represent the voltage drop across the heated foil. To minimize electrical contact resistance between the metallic heater foil and the copper bus bars (with its attendant undesirable heat dissipation during the tests) highly conductive nickel-based paint was applied between the heater foil and bus bars to reduce contact resistance.

Electrical current to the heater was recorded from the attached DC power supply and the voltage drop across the heater module was measured via the two leads. Power dissipated in the heater could then be calculated as the product of the measured voltage and current.

A single 0.051 mm diameter type T precision thermocouple was mounted directly to the underside of

the heated foil using epoxy. An electrical continuity check was performed to verify that the thermocouple was in intimate electrical contact with the foil. This guaranteed good thermal contact for the local temperature measurements. After the thermocouple was properly attached, the gap beneath the foil was filled with epoxy to protect it during submerged jet tests. Tests were performed to ensure that there was no electrical interaction between the thermocouple and the heated foil as follows. Temperature data were taken under typical experimental conditions. The polarity of the DC power supply was then reversed. The heat transfer coefficients determined from the measured temperatures under both polarity conditions differed by less than 5%. Such was the conclusion also in previous studies using a similar measurement technique with different apparatus [5, 12]. The jet exit liquid temperature was measured with a second thermocouple inserted into the tubing upstream of the nozzle.

Data acquisition

Voltages and thermocouple readings were measured using a HP-3421 data acquisition system with accuracy of 1 μV. This system was controlled by a HP-71 hand-held computer. The system was programmable to enable continuous sequential temperature readings necessary for the location of the stagnation point (point of minimum temperature), or single-point readings used in the investigation of nozzle-to-plate and radial variation measurements. The current drawn by the heater assembly was read directly from the DC power supply.

Experimental uncertainty

The uncertainty associated with the experimental data was estimated using a weighted root-sum-squared approach [13]. The results revealed maximum uncertainty in Reynolds and Nusselt numbers of 7.7 and 11.5%, respectively. The uncertainty in Nusselt number, dominated by the measurement of the temperature, was more typically 7–8%. As stated previously, the accuracy of the measured location of the heat transfer measurements is estimated at ± 0.013 mm.

The heat loss through the heater assembly substrate (epoxy layer) was analyzed numerically. The results revealed that these losses were less than 1% of the imposed Ohmic heat flux owing to the extremely high heat transfer coefficients at the jet-exposed surface. The analysis also showed lateral conduction in the heater foil to be negligibly small. Therefore, corrections to the data collected were unnecessary.

RESULTS AND DISCUSSION

Experimental data were gathered and analyzed in both free-surface and submerged liquid jet configurations. The results are presented and discussed separately with comparisons between the two configurations made where relevant.

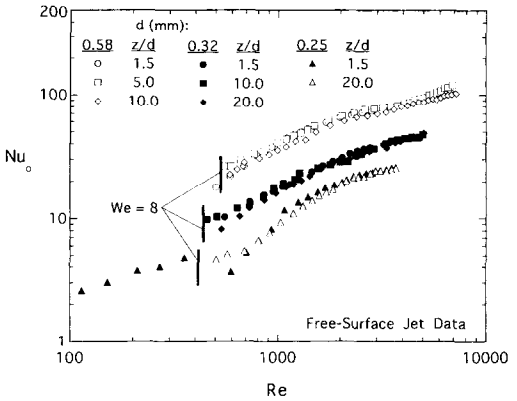

FIG. 3. Variation of stagnation Nusselt number with Reynolds number for the free-surface jet configuration.

Free-surface jet results

The variation of the stagnation Nusselt number with Reynolds number for select free-surface jet results is shown in Fig. 3. The figure illustrates that, despite nondimensionalization of the data, there is a distinct nozzle diameter dependence in the $Nu_0 \sim Re$ functional relationship; higher stagnation Nusselt numbers are observed for larger nozzle diameters. This same experimental observation has been made previously [5]. The Reynolds number corresponding to Weber number equal to eight is also shown in the figure. Below $We = 8$, and for large enough nozzle-to-plate spacing, the jet was observed to destabilize and break up in to droplets as a result of the surface tension. This observation is consistent with the analysis of Lienhard and Lienhard [14]. Limited data were taken below $We = 8$ only for very small z/d, under which conditions the droplet formation was inhibited and a continuous liquid stream was maintained. Examination of the data for the 0.25 mm diameter nozzle with $z/d = 1.5$ shows a discontinuity at $Re \approx 600$. This discontinuity was observed visually to occur as the radial location of the hydraulic jump, upon decreasing with reduced Reynolds number, finally disappears, leaving the tip of the nozzle slightly submerged.

The data of Fig. 3 reveal that the stagnation Nusselt number is nearly independent of nozzle-to-plate spacing, z/d. This is shown more completely in Fig. 4 for all three nozzle diameters studied. While the higher Re data in Fig. 4 show slight dependence of Nu_0 on Re at low z/d, generally the stagnation Nusselt number data exhibit negligible variation with nozzle-to-plate spacing for all diameters and over the full range of Reynolds number spanning initially laminar, transitional, and turbulent liquid jets. This observation is consistent with the conclusion of prior experimental studies of liquid jets at much higher Reynolds numbers, which reveal that the stagnation heat trans-

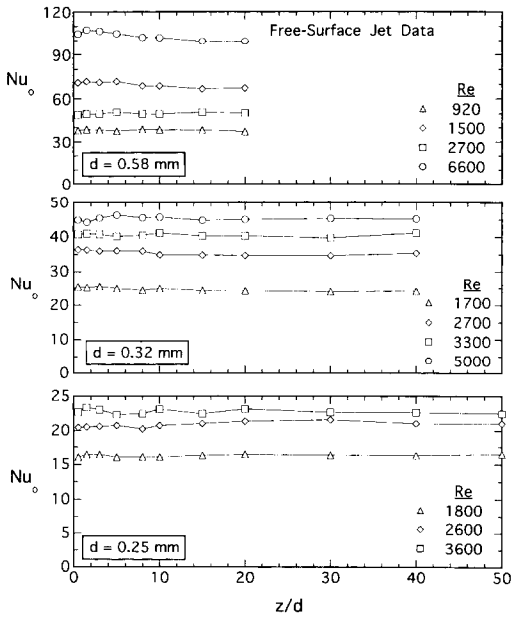

FIG. 4. Variation of stagnation Nusselt number with nozzle-to-plate spacing for the three nozzle diameters studied.

fer is not influenced by the spacing between nozzle exit and heated plate [5, 9].

The stagnation Nusselt number data of Fig. 3 are replotted in Fig. 5 as a function of both jet Weber number and Reynolds number. The figure reveals two relatively distinct regimes for the heat transfer coefficient data. The functional dependence of Nu_o on We and Re changes near $We \approx 200$ and $Re \approx 2000$, indicated by a change in the slope of the $Nu_o \sim We$

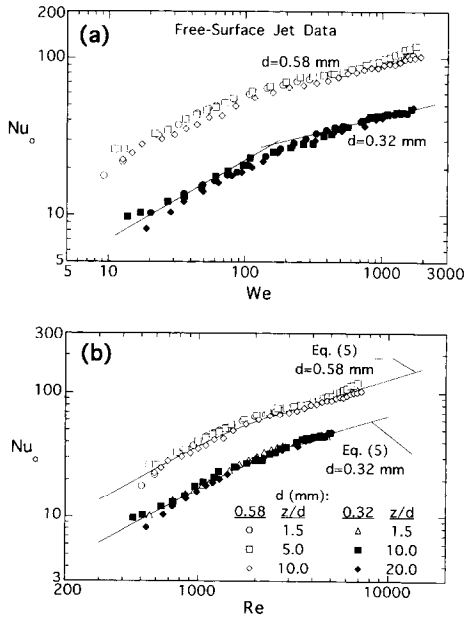

FIG. 5. Variation of stagnation Nusselt number with (a) Weber number, and (b) jet Reynolds number for the free-surface jets.

(shown by the faired lines in the $d = 0.32$ mm data) and $Nu_o \sim Re$ data there. These two regimes correspond loosely to the dominance of laminar and turbulent flow, respectively. The experimental data were correlated separately for the ranges $Re < 2000$ and $Re > 2000$ using the equation

$$Nu_o = aRe^b \tag{4}$$

where the coefficients a and b were determined from a least-squares regression of the data. The results of the regression analysis are summarized in Table 1 for the two regimes as a_{lam} and a_{turb}, b_{lam} and b_{turb}, respectively. The data for the 0.25 mm diameter nozzle were not correlated because of insufficient number of experimental points. Figure 5 and the coefficients of Table 1 indicate that the stagnation Nusselt number is more strongly dependent on Reynolds number for initially laminar free-surface jets, showing an approximate $Nu_o \sim Re^{0.8}$ relationship. The approximate $Nu_o \sim Re^{0.5}$ functional dependence reported previously for fully turbulent free-surface liquid jets [1–10] is also observed in this study.

Despite the transition from laminar to turbulent flow, the dependence of the stagnation Nusselt number on Reynolds number would be expected to be $Nu_o \sim Re^{0.5}$ predicted by laminar theory for stagnation flow due to the formation of an initially laminar boundary layer in the stagnation zone. The $Nu_o \sim Re^{0.8}$ relationship observed for $Re < 2000$ is therefore puzzling. Visual observation of the jet structure provides a possible explanation for the unusual heat transfer characteristics. The jets were imaged under magnification for the full range of Weber (Reynolds) number. The observations are summarized schematically in Fig. 6. For very low Weber number droplets begin to form at the nozzle tip and are torn off due to gravity (not shown). As the Weber number is increased the droplets coalesce into a single stream attached to the nozzle exit. The stream exhibits surface instabilities immediately downstream of the exit. The point of onset of these instabilities was observed to move downward along the jet as the Weber number was increased. (For all results reported here the point of onset of jet instability was beyond the nozzle-to-plate spacing investigated.) For both these low Weber number conditions just described (illustrated by the two low-We examples of Fig. 6) the liquid jet boundary coincided with the *outside diameter* of the nozzle tube due to surface tension effects. Thus, the jet itself was larger than the internal diameter of the nozzle. As the Weber number was increased the free-surface curvature at the nozzle exit increased and its diameter more nearly approached that of the internal dimension of the nozzle. Only at very high Weber (Reynolds) numbers did the jet issue from the nozzle tube at the same diameter as the internal nozzle dimension. Thus, for low We, the jet is broadened under the action of surface tension. This may explain the $Re^{0.8}$ dependence of the stagnation Nusselt number. Recall that Re was based on the

Table 1. Summary of laminar and turbulent correlation coefficients for free-surface and submerged liquid jets. The subscripts lam and turb indicate the jet regime for which the associated correlation coefficient is listed

Jet configuration	d (mm)	a_{lam}/a_{turb}	b_{lam}/b_{turb}	z/d range
Free-surface jets	0.58	0.109/1.75	0.847/0.465	<50
	0.32	0.0473/1.08	0.852/0.444	
Submerged jets	0.58	0.345/1.50	0.697/0.491	<8
	0.32	0.0955/0.963	0.781/0.473	
	0.25	0.0449/0.123	0.834/0.682	

liquid exit velocity and diameter. In reality, the jet diameter was larger at the nozzle exit for low We and the corresponding flow structure was therefore altered. The resulting modification of the velocity profile apparently happens immediately downstream of the jet exit, and prevails for the range of z/d studied as evident in Fig. 5. The anomalous $Nu_o \sim Re^{0.8}$ relationship below $We \approx 200$ ($Re \approx 2000$) corresponds to the regime where the jet was broadened due to surface tension, attaching itself to the nozzle tube outside diameter. The transition between the two regimes observed in Fig. 5 coincided with the Weber number where the jet momentum was high enough relative to surface forces that its exit diameter contracted to nearly match the internal diameter of the nozzle. It is only in the laminar range where surface tension effects are significant enough relative to jet momentum that a change in the structure of the jet results. The higher momentum and turbulent transport in the higher Re jets dominates the surface tension forces in this regime.

Using the dual-asymptote correlation technique of Churchill and Usagi [15], the separate Nusselt number descriptions for the initially laminar and turbulent jets were merged into a single expression representing both regimes. For convenience in its use in both regimes, the correlation is developed in terms of the Reynolds number, even though the Weber number is the appropriate governing parameter where surface tension effects are dominant. The relationship which describes both asymptotes observed may be stated

$$Nu_o = [(Nu_{o,lam})^{P} + (Nu_{o,turb})^{-P}]^{1/P} \quad (5)$$

where $Nu_{o,lam}$ and $Nu_{o,turb}$ are the stagnation Nusselt numbers correlated as a function of Reynolds number for the laminar and turbulent regimes, respectively, and are given by equation (4) and the associated coefficients in Table 1. The additional correlation coefficient, P, which appears in equation (5) is determined from an optimal fit of the data. Figure 5(b) illustrates the correlation of equation (5) for the $d = 0.32$ and 0.58 mm free-surface jet data using the value $P = 9$. The fit is quite good, representing the data spanning the jet range from initially laminar to fully turbulent flow at the jet exit.

The radial variation of the normalized local Nusselt number, Nu/Nu_o, for the free-surface liquid jet configuration is shown in Fig. 7 for two nozzle-to-plate spacings, $z/d = 1.5$ and 10 between $Re = 1300$ and 5500. The maximum heat transfer occurs in the stagnation zone and falls off with radial position; the heat transfer coefficient falls to 60% of its value at the stagnation point in a radial distance of just six diameters. Normalized by the value at the stagnation point, the radial variation in local heat transfer coefficient is

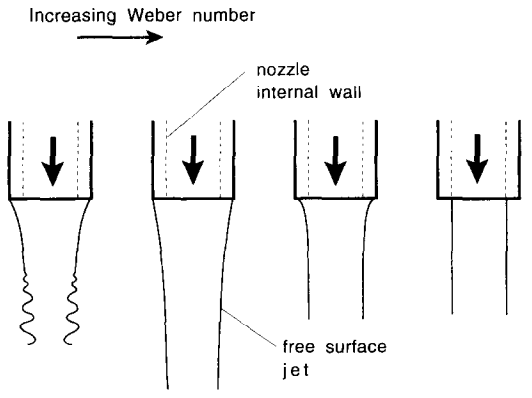

FIG. 6. Schematic illustration of observed free-surface jet structure with increasing Weber number.

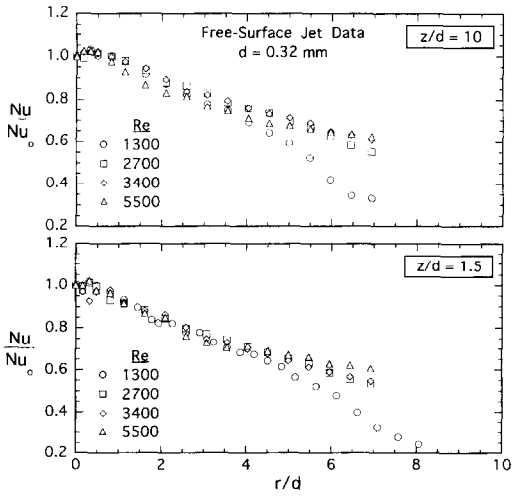

FIG. 7. Radial variation of normalized local Nusselt number for the free-surface jet configuration.

seen to be largely independent of Reynolds number for $r/d < 4$. At radial locations greater than 4 diameters, however, the Nusselt number for the initially laminar jet deviates from the turbulent flow data and exhibits a sharper decline with radial location. This is perhaps the combined result of the considerably lower momentum of the laminar jet relative to its turbulent counterpart, and turbulent mixing across the film for the high-Re cases. It may also be noted that the decay of Nu/Nu_0 with r/d appears to be slightly higher for lower nozzle-to-plate spacings. As will be seen shortly, this phenomenon is more pronounced in the submerged jet data. These data for $d = 0.32$ mm are representative of experimental results for the other nozzle diameters investigated [16].

Submerged jet results

The variation of the stagnation Nusselt number with Reynolds number is shown in Fig. 8 for the submerged jet configuration. Data are illustrated for all three nozzle diameters studied. As with the free-surface jet results, the stagnation Nusselt number data for the submerged jet illustrate two regimes corresponding to initially laminar and turbulent tube flow at the jet exit. The transition again appears to occur near $Re = 2000$. Below this critical Reynolds number the data for all nozzle-to-plate spacings collapse to a single band. Above this critical Reynolds number the data for the different nozzle-to-plate spacings investigated diverge; the data for higher z/d are lower than corresponding data at the same Reynolds number for nozzles closer to the heated plate. In fact, there is a transition between the laminar regime ($Re \lesssim 1500$) and the turbulent regime ($Re \gtrsim 1500$) where

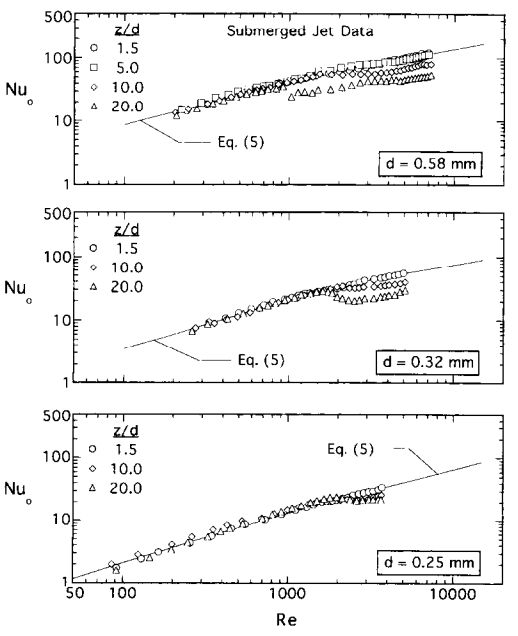

FIG. 8. Variation of stagnation Nusselt number with Reynolds number for the submerged jet configuration, and comparison with empirical correlation.

the Nusselt number actually decreases with increases in the Reynolds number. This is clearly evidenced in the $d = 0.32$ and 0.58 mm nozzle data for $z/d = 20$. This is presumably due to the higher shear and associated degradation of the jet approach velocity profile for jets which are initially turbulent. Those jets whose exit condition is laminar experience lower shear at their boundary because of the lower velocity gradients. Once the jet exit flow is fully turbulent, the well-established dependence of Nu_0 on z/d is seen. This dependence for fully turbulent submerged jets is the result of the formation of a velocity potential core [17]. As the nozzle-to-plate spacing is increased for initially turbulent jets, a local maximum in heat transfer coefficient is observed near $z/d = 8$, after which the transport behavior decreases. This value of z/d is loosely associated with the end of the potential core, where the jet approach velocity is not yet appreciably affected by shear, but where the turbulent transport is high.

As with the free-surface jet configuration, the submerged jet data were separately correlated in the laminar and turbulent flow regimes using the form of equation (4). The regression coefficient results are shown in Table 1. Since the stagnation Nusselt number for the submerged jet is dependent on nozzle-to-plate spacing the correlation was developed for $z/d < 8$, which is the end of the potential core for turbulent jets [17]. The dependence of the stagnation Nusselt number on nozzle-to-plate spacing will be documented in a section to follow. The stagnation heat transfer coefficient is relatively independent (variations typically less than 10–15%) for nozzle-to-plate spacings corresponding to $z/d < 8$. Again, a value of $P = 9$ was used in the composite correlation function, equation (5). The good agreement between correlation and experimental data is evident in Fig. 8.

Though nozzle-to-plate spacing is an important parameter for initially turbulent submerged jets, the data of Fig. 8 indicate it to be far less significant for initially laminar fully-developed jets. As was stated previously, the experimental data all merge to a single tight band as the Reynolds number is reduced below $Re \approx 2000$. Reynolds observed that submerged jets which are initially laminar experience destabilization and transition due to the shear layer interaction with the stagnant surrounding fluid [18]. This occurs somewhere between $Re = 10$ and 300. Hinze discusses the turbulent flow structure of initially turbulent submerged jets [19]. Experimental measurements reveal that, while the peak velocity decays with position along the centerline of the jet, the turbulence intensity increases. The data show that this increase in turbulence intensity increases dramatically between two and twelve diameters from the exit of the nozzle, with the change thereafter being relatively minor. One may speculate that this transition to turbulent flow of the jet penetrating the stagnant fluid may be delayed for submerged jets which are initially laminar. In terms of the stagnation heat transfer coefficient for such

jets, it may be suggested that the decay in approach velocity with the associated decrease in heat transfer is offset by jet destabilization and transition to turbulence with its associated increase in transport. The net effect for initially laminar jets is that seen in Fig. 8. The stagnation Nusselt number is relatively independent of z/d for $Re \leqslant 1500$ over the relatively broad range of nozzle-to-plate spacing investigated. This relative insensitivity of Nu_0 to changes in z/d for laminar jets has been observed previously for planar air jets [20].

The dependence of Nu_0 on z/d in combined laminar, transitional, and turbulent submerged jets is documented in Fig. 9. The stagnation Nusselt number, normalized by the Nusselt number measured at the minimum z/d examined experimentally, $Nu_{0,\min z/d}$, is plotted as function of nozzle-to-plate spacing for Reynolds numbers in the range $800 \leqslant Re \leqslant 6900$ for the three jet diameters studied. The data for low Reynolds number submerged jets reveal a relatively minor variation of Nu with z/d. In some cases the Nusselt number exhibits a slight increase with z/d for these laminar jets, perhaps due to the considerably higher transport characteristics of the unsteady jet after destabilization. By contrast, the fully turbulent jet exit condition data show a considerable decay in Nu beyond $z/d \approx 8$. This again supports prior observations and potential core-based explanations for fully turbulent jet impingement heat transfer [17]. Figure 9 shows that the decay in Nusselt number with nozzle-to-plate spacing increases with Reynolds number beyond $z/d \approx 8$. The influence of nozzle-to-plate spacing on Nusselt number is negligible for initially laminar submerged jets, and approaches the approximate $Nu_0 \sim (z/d)^{-1/2}$ dependence for turbulent jets described previously [8], and shown for comparison in the figure.

Figures 10 and 11 illustrate the variation in the local Nusselt number normalized by the stagnation Nusselt number for $d = 0.32$ and 0.58 mm, respectively. The dependence on z/d is shown for both sets of data. As was the case with free-surface liquid jet data of Fig. 7, the maximum heat transfer coefficient occurs in the stagnation zone and decreases thereafter with radial position. The same grouping of initially laminar versus initially turbulent jet data exists in the submerged jet data as well. The Nusselt number for the initially laminar jets decays more rapidly with radial location than the corresponding data for initially turbulent jets. This is presumably due to the higher transport characteristics of unsteady transport which exists at the stagnation zone and prevails radially outward in the turbulent jets. Also observed in the free-surface jet data of Fig. 7, the submerged jet data illustrate

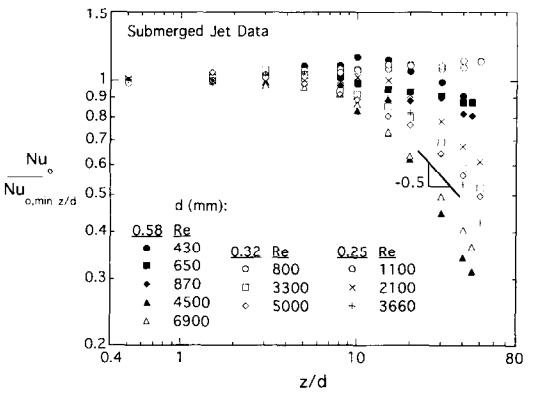

FIG. 9. Influence of nozzle-to-plate spacing on stagnation Nusselt number for submerged jets.

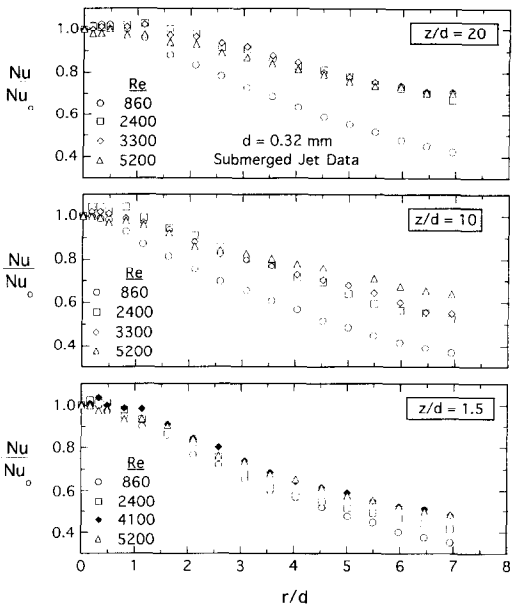

FIG. 10. Radial profiles of the normalized local Nusselt number for $d = 0.32$ mm.

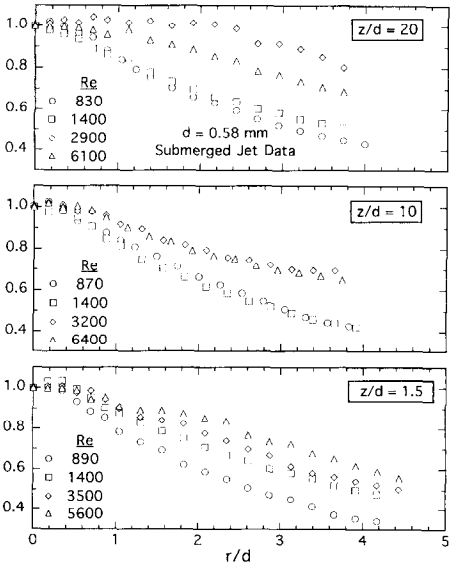

FIG. 11. Radial profiles of the normalized local Nusselt number for $d = 0.58$ mm.

that the radial decay in heat transfer coefficient is higher for smaller z/d. This is more pronounced for the submerged jet configuration, and is valid over the entire Reynolds number range.

Unique to the $d = 0.58$ mm data of Fig. 11 is a knee in the $Nu/Nu_0 \sim r/d$ curves at the two highest Reynolds numbers for $z/d = 1.5$. This occurs near $r/d = 2$, and has been observed in previous heat transfer studies of submerged gas and liquid jets, and has been explained as a possible transition to turbulent flow in the radial flow region [10, 21]. The data of this study show that the stagnation zone for $Re \gtrsim 2000$ heat transfer at the stagnation zone experiences a flow regime transition which corresponds to the laminar–turbulent transition in the jet tube flow. The possible transition in the radial flow region results in the near-secondary maxima which occur near $r/d = 2$.

Also of note in the $d = 0.58$ mm data of Fig. 11 is the anomalous variation in normalized Nusselt number with radial location for $Re = 2900$ at $z/d = 20$. The heat transfer coefficient is observed to be far less dependent on radial position for this set of experimental conditions. These data were reproduced several times to ensure repeatability. This unusual radial variation phenomenon was also observed with other nozzle diameters, always occurring at $z/d = 20$ and for Reynolds numbers in the range $2500 \leqslant Re \leqslant 3000$. This is illustrated more clearly in Fig. 12 which shows absolute (un-normalized) Nusselt numbers for $d = 0.25$ and 0.58 mm at $z/d = 20$. Data for Reynolds numbers which lie in the initially laminar and initially turbulent tube jet regimes display the usual behavior; the heat transfer coefficient is nearly constant in the stagnation zone and decays monotonically with radial location thereafter. The $d = 0.58$ mm data for $Re = 2900$ and the $d = 0.25$ mm data for $Re = 2600$ (connected by lines in the figure for clarity) exhibit far less variation with radial position. Further, the heat transfer coefficient for these Reynolds numbers do not show the monotonic increase with increasing Re found in profiles for other Re. For example, the $Re = 2600$ data for $d = 0.25$ mm is lower than the $Re = 1200$ case at low r/d, and higher at high r/d. It may be suggested that the transition to turbulent flow experienced by submerged jets with are initially laminar affects not only the stagnation zone heat transfer behavior, but also results in complex and rather anomalous variations in the local heat transfer coefficient with radial position.

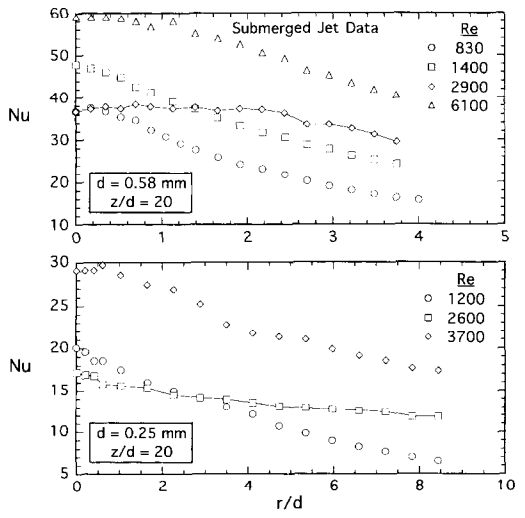

FIG. 12. Radial variation of absolute Nusselt number for $z/d = 20$.

CONCLUSIONS

Heat transfer from free-surface and submerged impinging liquid jets in the initially laminar, transitional, and turbulent flow regimes (at the nozzle exit) have been studied. Local heat transfer coefficient information was collected, and the radial variation of the Nusselt number is explored. The Nusselt number was observed to correlate approximately with $Re^{0.5}$ and $Re^{0.8}$ for initially turbulent and laminar jets, respectively, for both jet configurations. The $Re^{0.8}$ relationship for the laminar regime was explained in terms of surface tension-induced jet broadening and associated modification of the jet flow structure for free-surface jets. For the submerged jet configuration the $Nu_0 \sim Re^{0.8}$ laminar regime relationship is believed to be due to the increased turbulence associated with jet destabilization dominating the decay in approach velocity. As observed in previous studies of fully turbulent liquid jets, the free-surface configuration heat transfer data showed little dependence on nozzle-to-plate spacing. By contrast, the submerged jet data exhibit the usual potential core behavior for turbulent flow. The Nusselt number was seen to be independent of nozzle-to-plate spacing in the initially laminar jet regime. A rather complex dependence of Nu_0 on z/d was observed for transitional Reynolds numbers.

Acknowledgement—This work was supported in part by the U.S. National Science Foundation under Grant No. CBT-8552493.

REFERENCES

1. D. J. Womac, S. Ramadhyani and F. P. Incropera, Correlating equations for impingement cooling of small heat sources with single circular liquid jets, *ASME J. Heat Transfer* **115**, 106–115 (1993).
2. J. H. Lienhard V, X. Liu and L. A. Gabour, Splattering and heat transfer during impingement of a turbulent liquid jet, *ASME J. Heat Transfer* **114**, 362–372 (1992).
3. Y. Pan, J. Stevens and B. W. Webb, Effect of nozzle configuration on transport in the stagnation zone of axisymmetric impinging free liquid jets: Part 2. Local heat transfer, *ASME J. Heat Transfer* **114**, 880–886 (1992).
4. X. Liu, J. H. Lienhard V and J. S. Lombara, Convective heat transfer by impingement of circular liquid jets, *ASME J. Heat Transfer* **113**, 571–582 (1991).
5. J. Stevens and B. W. Webb, Local heat transfer coefficients under an axisymmetric, single-phase liquid jet, *ASME J. Heat Transfer* **113**, 71–78 (1991).
6. S. Faggiani and W. Grassi, Round liquid jet impinge-

ment heat transfer: local Nusselt numbers in the region with non-zero pressure gradients. In *Heat Transfer—1990, Proceedings of the Ninth International Heat Transfer Conference*, Vol. 4, pp. 197–202 Hemisphere, Washington, DC (1990).
7. D. J. Womac, G. Aharoni, S. Ramadhyani and F. P. Incropera, Single phase liquid jet impingement cooling of small heat sources. In *Heat Transfer—1990, Proceedings of the Ninth International Heat Transfer Conference*, Vol. 4, pp. 149–154. Hemisphere, Washington, DC (1990).
8. C. F. Ma, H. Sun, H. Auracher and T. Gomi, Local convective heat transfer from vertical heated surfaces to impinging circular jets of large Prandtl number liquids. In *Heat Transfer—1990, Proceedings of the Ninth International Heat Transfer Conference*, Vol. 2, pp. 441–446 Hemisphere, Washington, DC (1990).
9. C. F. Ma and A. E. Bergles, Convective heat transfer on a small vertical heated surface in an impinging circular liquid jet. In *Proceedings of the Second International Symposium on Heat Transfer*, Vol. I, pp. 248–255, Beijing, China (1988).
10. H. Sun, C. F. Ma and W. Nakayama, Local characteristics of convective heat transfer from simulated microelectronic chips to impinging submerged round water jets, *ASME J. Electron. Packaging* **115,** 71–77 (1993).
11. X. Liu, L. A. Gabour and J. H. Lienhard, V, Stagnation-point heat transfer during impingement of laminar liquid jets: analysis including surface tension, *ASME J. Heat Transfer* **115,** 99–105 (1993).
12. J. Stevens and B. W. Webb, The effect of inclination on local heat transfer under an axisymmetric, free liquid jet, *Int. J. Heat Mass Transfer* **34,** 1227–1236 (1991).
13. T. G. Beckwith, N. L. Buck and R. D. Marangoni, *Mechanical Measurements* (3rd Edn). Addison–Wesley, Reading, MA (1982).
14. J. H. Lienhard V and J. H. Lienhard IV, Velocity coefficients for free jets from sharp-edged orifices, *ASME J. Fluids Enging* **106,** 13–17 (1984).
15. S. W. Churchill and R. Usagi, A general expression for the correlation of rates of transfer and other phenomena, *A.I.Ch.E. Jl* **18,** 1121–1128 (1972).
16. B. Elison, Submerged and free-surface liquid jet impingement heat transfer for fully developed laminar and transitional flows, M.S. Thesis, Brigham Young University, Provo, Utah (1993).
17. H. Martin, Heat and mass transfer between impinging gas jets and solid surfaces. In *Advances in Heat Transfer* (Edited by J. P. Hartnett and T. F. Irvine), Vol. 13, pp. 1–60. Academic Press, New York (1977).
18. A. J. Reynolds, Observations of a liquid-into-liquid jet, *J. Fluid Mechanics* **14,** 552–556 (1962).
19. J. O. Hinze, *Turbulence* (2nd Edn). McGraw-Hill, New York (1975).
20. E. M. Sparrow and T. C. Wong, Impingement transfer coefficients due to initially laminar slot jets, *Int. J. Heat Mass Transfer* **18,** 597–605 (1975).
21. R. Gardon and J. C. Akfirat, The role of turbulence in determining the heat transfer characteristics of impinging jets, *Int. J. Heat Mass Transfer* **8,** 1261–1272 (1965).